Primitive Path Networks Generated by Annealing and Geometrical Methods: Insights into Differences

Sachin Shanbhag*,†,‡ and Martin Kröger§,||

School of Computational Science, Florida State University, Tallahassee, Florida 32306-4120, Department of Chemical and Biomedical Engineering, FAMU-FSU College of Engineering, Tallahassee, Florida 32310-6046, and Polymer Physics, Department of Materials, ETH Zurich, Wolfgang-Pauli-Strasse 10, CH-8093 Zurich, Switzerland

Received October 24, 2006; Revised Manuscript Received January 10, 2007

ABSTRACT: Existing methods to obtain the primitive path network for monodisperse, linear polymers in the molten state are critically compared. A connection is established between the original "annealing" and newer geometrical approaches. A discrepancy of about 15% is observed in the mean primitive path length obtained by these methods for well-entangled polymers. This deviation is attributed to disentanglement that occurs during annealing. A number of well-equilibrated polymeric systems and some toy-configurations (rings) were studied to estimate the relative contributions of slip and constraint release by end-looping to the observed disentanglement. We found that about half ($\approx$ 7.7%) of the discrepancy persists for ring polymers in which end-looping is not possible, and may be attributed to slip alone. It is argued that the characteristics of the network obtained by annealing become practically equivalent to those obtained by geometrical methods in the asymptotic limit of small chain diameter and rapid quenching.

Introduction

In concentrated polymer solutions or melts, the volume occupied by a single polymer chain is pervaded by several other molecules. It produces topological interactions and some of the persistent contacts constrain the mobility of the chains. Such topological constraints are commonly called "entanglements". The primitive path of a polymer chain immersed in a sea of obstacles is defined as the shortest path connecting the ends of the chain that does not violate the topolgical constraints imposed on it.[1] The ideas of primitive paths (PP) and entanglements are fundamental to our understanding of concentrated polymer solutions and melts, and distinguish them from unentangled polymer solutions. The dominant mean-field theory, called the "tube model",[1] and its numerous refinements explain some of the phenomenology associated with entangled linear polymers.[1−8] It models polymer dynamics in a self-consistent manner by representing chains as Gaussian PPs. Similarly, assumptions about the PP network form the starting point for stochastic descriptions such as "slip-link" models, which are able to explain the rheology and dielectric relaxation in linear and branched polymer melts.[9−18]

Recently, Everaers et al.[19] suggested a simulation algorithm called "annealing" based on the idea put forward by Rubinstein and Helfand[20] to construct the underlying PP network, starting from a well-equilibrated system of densely packed polymers. In this method, the ends of all the chains are immobilized and intrachain excluded volume is switched off, while interchain excluded volume is retained. As the temperature of the system is gradually reduced to zero, the tension in the chains irons out the excess slack in the all the chains simultaneously. In particular, Everaers et al. showed that the above definition of the primitive path agrees with the entanglement density that yields the experimentally observed height of the plateau modulus. The report by Everaers et al. inspired several other efforts that adapted the spirit of the annealing algorithm to lattice simulations,[21] and used alternative geometrical methods to obtain the PP network.[22,23] The excitement caused by this recent body of work is understandable as these developments constitute the missing bridge between mean-field tube theories, and slip-link models on the one hand and microscopic descriptions via molecular dynamics (MD) or lattice Monte Carlo (MC) methods[24,25] on the other. The nonuniqueness or degeneracy of the resulting PP network has been recognized,[22,26,27] and several new subjects such as the role of self-entanglement,[28] the difference between energy minimization and length minimization,[21,26] the location of entanglement points along a PP,[22,23,27] PP statistics,[8,22,23,27,29] and the validity of assumptions made in slip-link and tube models such as the chain retraction potential and the dilution exponent have been examined.[21,27,29]

Thus, to date, four different methods to extract the PP network from a simulation snapshot have been proposed:

(A) "annealing" method[19,26,28] ($\Sigma \approx 1000$);

(B) lattice MC-adapted annealing method[21,27] ($\Sigma \geq 100$);

(C) shortest multiple disconnected path approach or the "Z-code"[22,29] ($\Sigma \approx 1$);

(D) the contour reduction topological analysis approach or "CReTA"[23] ($\Sigma \geq 10$).

Here, Σ is the total computing time per particle in units of centiseconds on a modern processor. Methods B−D seek to minimize the total contour length, while method A tends to minimize the model-dependent total energy,[19,28,30] or alternatively, the total path length[26] of the system, by altering the spring law that regulates the tension in the chain during annealing. Methods C and D consider, in principle, infinitely thin paths without the need to introduce spring or excluded volume interaction potentials. It is important to note that these minimization goals are reached subject to constraints, which

* Corresponding author. Present address: School of Computational Science, Dirac Science Library, Florida State University, Tallahassee, FL 32306-4120. Telephone: 850.644.6548. E-mail: sachins@scs.fsu.edu.

† School of Computational Science, Florida State University.

‡ Department of Chemical and Biomedical Engineering, FAMU−FSU College of Engineering.

§ Polymer Physics, Department of Materials, ETH Zurich.

|| E-mail: mk@mat.ethz.ch.

10.1021/ma062457k CCC: $37.00
Published on Web 03/24/2007

aim to preserve the state of physically relevant entanglements. Otherwise, the system would disentangle completely and the shortest path, or deepest energy state, would yield straight-lines between chain-ends. All the four methods work in discontinuous time and coordinate space; i.e., they use discrete time steps and finite displacements during which disentanglement processes need to be avoided. Methods C and D deal with uncrossable bead-connecting segments rather than excluded volume multibead chains as relevant objects. They prevent disentanglement by constraining moves of kinks (nodes) on the shortest path to (i) lie in the plane spanned by its two adjacent segments (edges), and (ii) to strictly shorten the path length. Methods C and D are essentially parameter-free. Methods A and B operate on multibead chains and are characterized by substantial chain slippage which results from the need to soften the effect of excluded volume interactions. Finally, the methods differ in their computational efficiency, although all of them scale linearly with system size. The total computing time per particle, proportional to Σ, differs by 3 orders of magnitude.

To summarize, the annealing methods A and B require the specification of several parameters such as the annealing time, strength, excluded volume interaction and bead−spring characteristics. In contrast, the "athermal" geometrical methods strictly prevent disentanglement, are parameter-free, and minimize length rather than energy. Given their computational efficiency, it is likely that they will replace the annealing methods, once a relationship has been established in detail.

In the best scenario, the properties of consequence would be insensitive to subtle differences in the PP networks obtained by using different methods. While this has borne out, at least semiquantitatively, for some properties such as the distribution of entanglement points, and PP segment length using three different methods, namely the Z-code,[29] CReTA,[23] and a lattice-based enumeration algorithm,[27] other data such as the width of the distribution of PP lengths indicate, however, that one cannot expect this to hold in general.[26] A logical step in this development would be to compare some of the existing methods more closely, preferably by using them on the same set of equilibrated systems. It is in their differences that important lessons lie waiting to be discovered. In this paper, we describe a more universal and efficient version of the previously reported Z-code, which will henceforth be called Z1.[22,29] We will compare this algorithm with the annealing method developed for lattice simulations.[27]

Model and Methods

In order to generate configurations, we use Shaffer's version of the bond-fluctuation model (S−BFM), which is a variant of the original bond-fluctuation model (BFM) proposed by Carmesin and Kremer.[31] N_p polymer chains, each consisting of N monomers or beads, are grown as self-avoiding random walks placed on a regular 3D cubic lattice. The reasons for choosing S−BFM over the original BFM, the methods used to equilibrate, anneal and specify the location of entanglement points using the identification of local deviations (ILD) technique have been described in detail in previous publications.[21,27] The systems of equilibrated polymer melts considered for PP analysis here have been reported in an earlier publication.[27] Table 1 provides a summary of these systems. The following discussion in this section may be skipped or quickly scanned by readers who are familiar with methods A to D. Besides recapitulating these methods, it indicates how we accelerated method B to arrive at $\Sigma \approx 100$, and explores its "quenching"mode. The section concludes with a summary of differences between the Z and Z1-codes.

Annealing (Methods A and B). Shanbhag and Larson[21] adapted the annealing algorithm originally proposed by Everaers et al. to compute the PPs of equilibrated chains for lattice MC simulations.[19] The idea is to facilitate the shrinkage of the chain contours which nevertheless maintain their noncrossability with other chains. The acceptance probability with which moves that increase the PP length is dialed down according to the expression, $p_{acc}(t) = \min\{1, \exp[-A\Delta L(t/\tau_A)^2]\}$, where ΔL is the change in contour length (positive or negative) due to a trial move, and τ_A is the duration of the annealing process. Thus, A and τ_A serve as two independent parameters.

Table 1. Description of the Systems Simulated, and Ensemble-Averaged Primitive Path Length Obtained by Annealing ($L^{(A)}_{ppA}$), Z1 (L_{ppZ}), and Annealing Followed by Z1 ($L^{(A)}_{ppA\to Z}$)[a]

N	N_p	$\langle R^2\rangle$	$\langle L^{(16)}_{ppA}\rangle$	$\langle L_{ppZ}\rangle$	$\langle L^{(16)}_{ppA\to Z}\rangle$	$\langle L^{(16),}_{ppA}*\rangle$
32	244	71.8	11.0	10.6	9.4	11.0
75	285	174.3	23.2	21.5	18.8	18.3
125	364	337.2	37.3	34.7	29.9	36.7
300	277	732.6	85.5	77.8	66.8	71.7
500	216	1189.3	140.4	125.6	107.0	116.6

[a] $L^{(A)}_{ppA}*$ was calculated after connecting entanglement points obtained via ILD with straight-line segments to partially offset the effect of the lattice. The annealing parameters used were $A = 16$ and $\tau_A = 10\tau_R$. Lengths are reported in lattice units.

In our previous simulations,[21,27] we set $A = 16$, and $\tau_A \approx 10\tau_{Rouse}$, where τ_{Rouse} is the Rouse relaxation time. This choice implies that $p_{acc} = 1/e$ when $t/\tau_A = 1/4$ for $\Delta L = +1$. For a polymer melt with fractional occupancy of lattice sites $\phi = 0.5$, the Rouse time of an entanglement segment $\tau_e \approx 5000$ Monte Carlo steps (MCS). Since $\tau_{Rouse} = \tau_e N^2$, $\tau_A = 50\,000 \times N^2$. We reported earlier that increasing τ_A or varying A between 10 and 20 had a negligible effect on properties such as mean PP length $\langle L_{pp}\rangle$ (which we denote by $\langle L_{ppA}\rangle$ when it is obtained using the annealing method) and the distribution around this mean.

In the limit of fast cooling $A \to \infty$, the acceptance probability becomes $p_{acc} = 0$ and $p_{acc} = 1$ for $\Delta L > 0$ and $\Delta L \le 0$, respectively. We label this limit, in which moves that increase the contour length are rejected, as "quenching". As remarked elsewhere,[27] in this limit the system often gets stuck in local minima, which it cannot jump out of, since increases in $\langle L_{ppA}\rangle$ are prohibited. As we will argue later, entrapment in a local minima occurs due to the size of the repulsive beads which impose a tangential structure. Methods A and B in their quenching mode return, by construction, results comparable with methods C and D in the limit of vanishing bead size along the polymer backbone.

To identify the spatial location of individual entanglements, the "local" structure of the PP has to be examined. The basic idea is the observation that if the length of a small segment of the PP deviates from the shortest path connecting its ends, the presence of a topological constraint in that neighborhood which prevents the PP segment from shortening its length may be inferred. Shanbhag and Larson[27] argued that the smallest such element which could be examined was three consecutive PP monomers, or two consecutive bonds. Thus, they hypothesized that if the trajectory of the PP between a bead and its second-nearest neighbor does not follow the shortest possible path along the cubic lattice, it is due to an obstacle or entanglement. They showed that this natural choice led to good agreement with the average number of entanglements Z calculated according to the expression $Z = \langle L_{ppA}\rangle^2/\langle R^2\rangle$, which assumes that chains are Gaussian coils. This method will be referred to as the identification of local deviations (ILD) method.

Effect of Annealing Parameters. In order to explore the possibility of accelerating the annealing procedure with more aggressive choices of A and τ_A, we varied the parameters A and τ_A over a wide range, and monitored the decrease in $\langle L_{ppA}\rangle$ as a function of time during the annealing procedure. We considered a well-entangled system from Table 1, viz. $N = 300$. In this analysis, $\langle L_{ppA}(t = 0)\rangle$ denotes the average contour length of the equilibrated chains just before annealing, and $\langle L_{ppA}(t = \tau_A)\rangle = \langle L_{ppA}\rangle$ is the mean PP length at the end of the cooling process. In the inset of Figure 1, the parameter $A = 16$ was held fixed, while τ_A was varied from τ_e

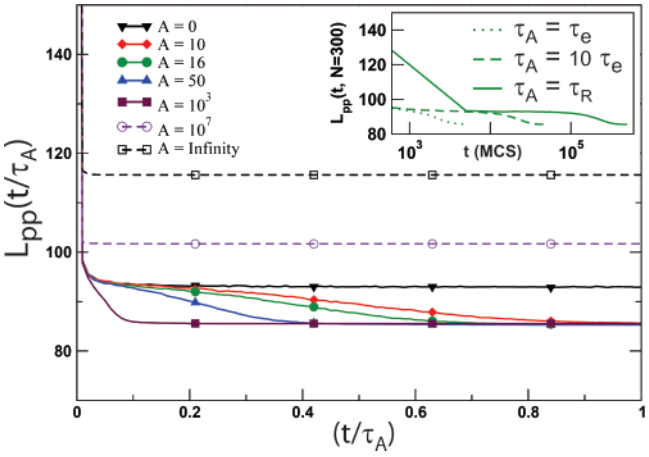

Figure 1. Effect of annealing parameters ($N = 300$). Decrease in the contour length $\langle L_{ppA}^{(A)} \rangle(t)$ during the annealing process, with $\tau_A = 5\tau_e$, and varying values of A. The inset shows $\langle L_{ppA}^{(16)} \rangle$ during the annealing process, with τ_A as the variable parameter.

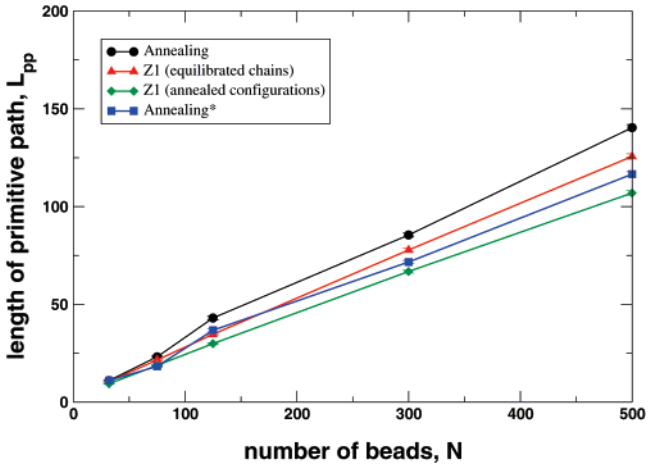

Figure 2. Average primitive path length $\langle L_{pp} \rangle$ obtained from an equilibrated melt using annealing (circles) and Z1 (triangles). The entanglement points on a PP obtained via ILD were connected by straight-line segments to partly compensate for the effects of the lattice. This measure is denoted by squares. When the annealed PP network was provided as input, instead of the equilibrated chains, to Z1 the $\langle L_{pp} \rangle$ decreased further (diamonds) by about 15%.

to τ_{Rouse}. The average contour length before the commencement of the annealing procedure was $\langle L_{ppA}(t = 0) \rangle = 421.2 \pm 0.2$. The values of $\langle L_{ppA}(t = \tau_A) \rangle$ were 85.8 ± 1.0, 85.5 ± 1.0, and 85.6 ± 1.0 when τ_A was set to τ_e, $10\tau_e$, and τ_R, respectively. All these results are within the standard error of mean of the $\langle L_{ppA} \rangle$ reported in Table 1 for which $\tau_A \approx 10\tau_{Rouse}$ was used. Besides the average $\langle L_{ppA} \rangle$, the distributions of PP lengths were also indistinguishable. Thus, the τ_A used previously was overly conservative. The computational load would have been reduced by about 2 orders of magnitude or more for well-entangled systems, had we used $5\tau_e < \tau_A < 10\tau_e$ instead. In Figure 1, we considered the same system, and held τ_A fixed at $5\tau_e$. The parameter which controls the rate of cooling A was varied. A small value of A corresponds to a gradual rate of cooling, and as $A \rightarrow \infty$, the limit of quenching is approached. For "moderate" values of A between 10 and 1000, the average PP length converges to approximately the same value of $\langle L_{ppA} \rangle \approx 85.5$ (see Figure 1). We observe a precipitous decrease in $\langle L_{ppA}(t) \rangle$ initially ($t < 0.02\tau_A$), which appears to be independent of A. For $A = 0$, the acceptance probability of a MC trial move is unity regardless of whether that move increases or decreases the total PP length, so long as it satisfies the interchain excluded volume, chain connectivity and uncrossability criteria. Thus, the initial decrease in $\langle L_{ppA}(t) \rangle$ stems largely from the relaxation of intrachain excluded volume irrespective of intermolecular arrangement. For moderate values of A, we discern a subsequent regime in which $\langle L_{ppA}(t) \rangle$ decreases at a slower rate, with the decrease being more gradual for smaller values of A. In this phase, the bias applied through $p_{acc}(t)$ manifests itself. As discussed later, for much larger values of A, a qualitatively different picture emerges.

Z-Code and CReTA (Methods C and D). While the annealing method A uses a small time step and moves beads simultaneously according Newton's equations that are coupled to a thermostat, the "athermal" geometrical codes (methods C and D) use the maximum possible time step, quite in the spirit of a constrained steepest descent method. They move beads sequentially, along polymer backbones (Z-code, and CReTA) or in space (Z1, in which spatial resolution decreases with time). The Z-codes and CReTA prevent disentanglement by constraining moves of kinks to lie in the plane of their adjacent segments. They can use a large "time step" since a single kink moves at a time. In practice, several kinks move at the same time while leaving the length of the shortest path strictly unchanged. Both Z- and Z1-codes do not operate with a constant number of beads, rather, they use kinks originally located at bead positions that tend to disappear during the minimization process, to speed up computations. The multiple disconnected path length of the system is thus strictly decreasing and corresponds to a quenching mode in the language of annealing algorithms. It does not get stuck before reaching the final state because the path is structureless. The Z-codes yield comparable results as long as the system size is large compared to the maximum end-to-end distance and the chosen line thickness is not too small. Otherwise, the original Z-code may fail and the Z1-code has to be used. This agreement alone is a hint that the sequential order of moves does not play a major role in determining the network. The Z1-code removes the above-mentioned restrictions in the applicability of the Z-code strategy. The CReTA approach (method D) is similar in spirit and preserves, in addition, information about distances between atomistic beads and their final position on the primitive path at the cost of preserving the initial number of beads. Compared to Z1, it results in a more gradual decrease of path length. Chain thickness issues have been discussed in Tzoumanekas and Theodorou.[13,23]

Results and Discussion

Comparisons between the Z1 and Annealing Algorithms. To perform this analysis, we considered all the systems reported in Table 1, which span the range from lightly entangled to well entangled melts.[27] The annealing parameters used to obtain the $\langle L_{ppA} \rangle$ in Table 1 were $A = 16$, and $\tau_A = 10\tau_{Rouse}$. Subsequently, we applied the ILD algorithm to the resulting PP network to identify the locations of entanglement points along the PP. For comparison, we also applied the Z1 code to the same set of systems.

Figure 2 depicts the average PP lengths $\langle L_{ppA} \rangle$ and $\langle L_{ppZ} \rangle$ obtained by annealing and Z1, respectively. For entangled systems, especially for $N \geq 125$, we observe a linear dependence of $\langle L_{pp} \rangle$ with N, as expected. The PP length obtained by Z1, $\langle L_{ppZ} \rangle$, is systematically smaller than that obtained by annealing, $\langle L_{ppA} \rangle$, at given N. In the lattice MC implementation of the annealing algorithm, the beads comprising the PPs are forced to remain on lattice sites. Thus, the coarse-grained nature of the lattice is partly responsible for this inequality. The effect of the grid can be filtered out to a first approximation by connecting with straight-line segments the entanglement points identified by ILD, on PPs generated by annealing. The agreement between the average PP length of the PP network thus constructed $\langle L_{ppA}^{*} \rangle$ and $\langle L_{ppZ} \rangle$ is slightly better (see Figure 2). We also note that in contrast with $\langle L_{ppA} \rangle$, $\langle L_{ppA}^{*} \rangle$ is smaller than $\langle L_{ppZ} \rangle$.

Given a well-equilibrated system, the common objective of the annealing and Z1 algorithms is to minimize $\langle L_{pp} \rangle$ subject to constraints and yield the corresponding PP network. If the

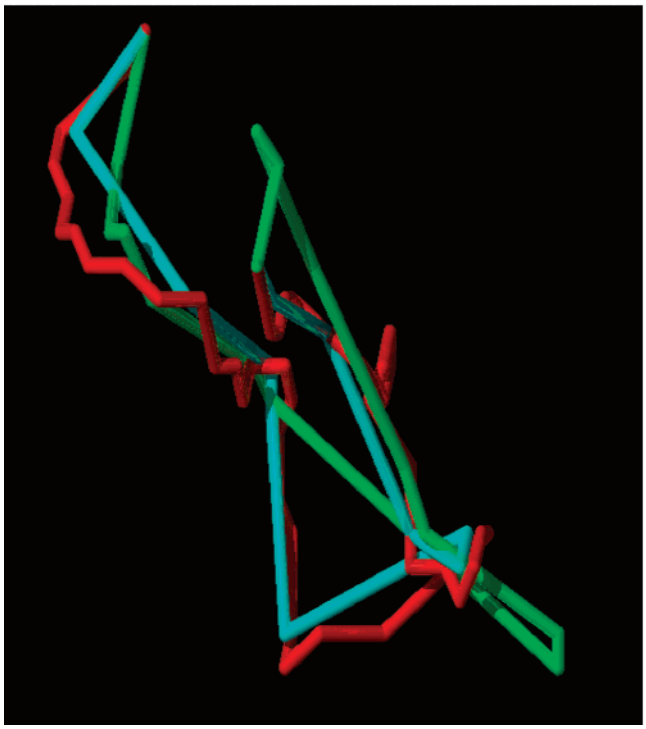

Figure 3. PPs of a single chain obtained using different methods. The red and green PPs were generated using Z1 and annealing, respectively. The red PP is jagged because it is forced to conform to the lattice. The cyan PP was obtained by applying Z1 on the previously annealed system. The fact that the annealed network is altered by the geometric code contains the important information that the methods produce different results except in a limiting case of small chain diameter and rapid quenching.

resulting PP network is supplied as input to the Z1 or annealing algorithms, we expected the output to remain essentially unchanged, since the objective function (total contour length) has already been minimized in the starting configuration. Indeed, this expectation was confirmed independently for both Z1 and annealing (both methods are designed as "projectors"). We provided the PP network obtained by annealing as input to Z1, anticipating that the resulting average PP length would be equal to $\langle L_{ppZ}\rangle$. To our surprise, we found that $\langle L_{ppA\rightarrow Z}\rangle < \langle L_{ppZ}\rangle$ systematically, where $\langle L_{ppA\rightarrow Z}\rangle$ represents the average PP length when the annealed configuration is provided as input to Z1. This additional decrease in the value of $\langle L_{pp}\rangle$ was of the order of 15% (see Table 1). The reverse process, in which the starting configuration for annealing is the output of Z1, cannot be implemented in general because the unique mapping from off-lattice co-ordinates onto a lattice requires a grid spacing that is small compared to the smallest distance within the network produced by Z1. The fact that the annealed network is altered by the geometric code contains the important information that the methods produce, except in a limiting case that we will see later, different results for primitive path lengths (not merely minor differences in networks characteristics, with the same average path length, as one may expect).

In Figure 3, the PPs obtained using three different methods mentioned above are depicted for a representative chain with $N = 300$. It supports the hypothesis that partial disentanglement occurs during annealing. The PP generated using annealing (red chain) seems to "obey" the same set of topological constraints as the PP that is generated by operating Z1 on the annealed configuration (cyan chain). In contrast, the PP generated by Z1 (green chain in Figure 3) acting on the equilibrated system appears to obey a different set of constraints. On average, the

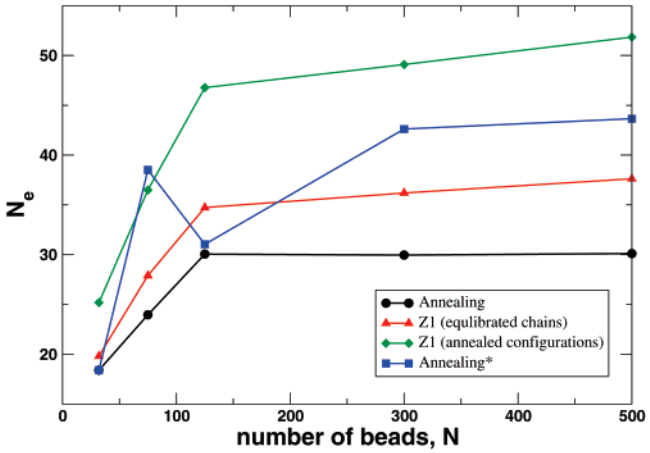

Figure 4. Average number of beads per entanglement N_e, which depends on the method used to obtain the underlying primitive path network. The values of $N_e = (N-1)\langle R^2\rangle/\langle L_{pp}\rangle^2$ were obtained by using the average properties reported in Table 1 and Figure 2.

PPs constructed by this process are longer and encounter a larger number of entanglements. Figures 2 and 3, taken together, strongly suggest that at least some of the entanglements preserved by Z1 are lost or released during annealing. This can be discerned from Figure 4, which depicts the number of monomers between entanglements N_e, which is related to the average properties reported in Table 1 via $N_e = (N-1)\langle R^2\rangle/\langle L_{pp}\rangle^2$. For chains of a given length, a larger value of N_e implies a more sparsely entangled network. Depending upon the method used to compute $\langle L_{pp}\rangle$ (columns 4−7 in Table 1), we have four different measures of N_e. The values of N_e vary from $N_e \approx 30$ for annealing to $N_e \approx 50$ for annealing followed by Z1. Some reference values obtained by different methods are available in literature.[18,32,33] We observe an approximately 30% difference in N_e obtained by Z1, depending on whether the equilibrated system or the PP network is fed as the starting configuration. Since Z1 prevents disentanglement, we attribute the dilution of the entanglement density to annealing.

This still leaves us with an unanswered question: what is the mode by which entanglements are lost during annealing? Annealing and Z1, as elaborated earlier, differ considerably in their respective implementations. However, there are two essential physical differences in the processes that these two methods model that are responsible for the partial disentanglement observed during annealing, namely *chain slip* and *end-looping*. Unlike Z1, the friction between chain contours is not infinite (chains are not "sticky") in the annealing algorithm and they can slip or slide over one another. In addition, it is possible for chain contour lengths to increase during annealing. This results in the phenomenon of constraint release by end-looping (CR-EL) which was recently visualized by Zhou and Larson[34] in the context of "tube-sampling", where they carried out MD simulations of a concentrated system of polymer chains whose ends were immobilized. In the annealing process, such end-looping moves are certainly possible, especially at early times, although we expect their occurrence to become less frequent as annealing proceeds, since the availability of sufficient slack required to form a loop becomes vanishingly small. For the sake of completeness, we note that at nonzero temperatures end-looping is possible during annealing without the formation of a "loop" (although the contour length still has to increase), especially for entanglements that are close to a chain end, as shown in Figure 5. Thus, for linear chains, the mechanisms of end-looping and slip are not completely independent. In the next section, we decouple these two mechanisms by looking at a

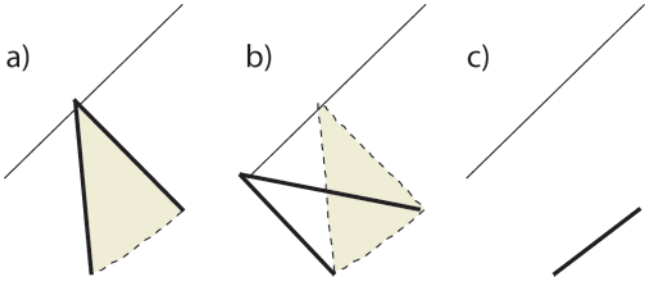

Figure 5. Out-of-secant area disentanglement process without slack which may occur during annealing at finite temperatures where chain slip is present. The Z-codes and CReTA leave configuration a unchanged because the kink cannot leave the secant area (shaded region surrounded by dashed line).

system of entangled rings in which end-looping cannot transpire and differences in PP network characteristics arise exclusively due to slip. We also study annealed networks obtained by quenching in which moves that increase the contour length are strictly prohibited. This study points us to an asymptotic limit in which the annealing and geometrical methods become formally equivalent.

Disentanglement during Annealing. Earlier in the paper (see Figure 1), we discussed the dependence of $\langle L_{\mathrm{ppA}} \rangle$ on the parameter A and showed that for moderate values of A the terminal $\langle L_{\mathrm{ppA}}(t = \tau_{\mathrm{A}}) \rangle$ was independent of A. We also showed that most of the contour-length reduction occurs quickly, while $t/\tau_{\mathrm{A}} < 0.02$ (see Figure 1). Further, by inspecting the $\langle L_{\mathrm{ppA}\to\mathrm{Z}} \rangle$ column in Table 2 it is evident that the level of disentanglement is unaltered as A increases from 0 to 1000. This is reasonable since CR-EL is more likely in the initial phase when sufficient chain slack is available to form loops. Thus, the observed loss of entanglements has manifested itself during the steep initial decrease in $\langle L_{\mathrm{pp}} \rangle$, where $At^2/\tau_{\mathrm{A}}{}^2 \ll 1$. To examine what happens in the short initial phase where $t/\tau_{\mathrm{A}} \approx 0.02$, we increased A beyond $1/(0.02)^2 \approx 2500$. From Table 2, we notice that the difference between $\langle L_{\mathrm{ppZ}} \rangle$ and $\langle L_{\mathrm{ppA}\to\mathrm{Z}} \rangle$, which is a measure of the level of disentanglement, decreases. When moves that increase contour length are strictly rejected during annealing (quenching, or zero-temperature annealing), the gap between Z1 and annealing begins to close, as clearly demonstrated by Table 2. Figure 7 depicts the starting and final configurations of a representative chain with $N = 300$ picked from the system described in Table 1, when Z1 is employed. It is clear from the figures that at least one entanglement that is preserved during quenching ($A \to \infty$) is lost during a slower annealing run with $A = 16$ due to end-looping.

Slippage during Annealing. To isolate the effect of chain-slip, and to understand quantitative differences in path lengths which are also present, but not caused by disentanglement, we constructed a special system in which disentanglement by such moves was forbidden by design. Such a system consisting of a series of concatenated or "Olympic" rings is shown in Figure 6. The average number of beads on the rings is approximately $N = 190$, with an average initial contour length of $L = 204.4$. To prevent the global drift of the system during annealing, the "first" and "last" beads (which are always adjacent) were fixed in space, similar to linear chains. Obviously, due to the bond between these two beads, the system cannot disentangle completely under any circumstance. Using methods described earlier, we found that for this system $\langle L_{\mathrm{ppA}} \rangle = 108.7$, $\langle L_{\mathrm{ppZ}} \rangle = 106.3$, and $\langle L_{\mathrm{ppA}\to\mathrm{Z}} \rangle = 98.1$. Therefore, even in this system, there is a further reduction in $\langle L_{\mathrm{ppZ}} \rangle$. However, this difference between $\langle L_{\mathrm{ppZ}} \rangle$ and $\langle L_{\mathrm{ppA}\to\mathrm{Z}} \rangle$ is $\approx 7.7\%$ for rings, which is about half the difference between the same quantities for linear chains. Figure 6 shows the configurations at the start and end of the different methods to identify the PP network. During annealing, the entanglement point between chains slides along chain contours seeking to minimize $\langle L_{\mathrm{pp}} \rangle$. This is borne out in the figure, where $A \to \mathrm{Z}$ filters out the effect of the grid by straightening the annealed path. Therefore, the observed discrepancy between $\langle L_{\mathrm{ppZ}} \rangle$ and $\langle L_{\mathrm{ppA}\to\mathrm{Z}} \rangle$ arises due to slip alone. While disentanglement, as described by dilution of the entanglement density, does not occur in this example, it illustrates how chain slip can alter the characteristics of the PP network that is generated.

Limiting Equivalence between Geometric and Annealing Approaches. The geometric methods C and D essentially operate as follows. They pick two adjacent segments $\mathbf{u}_{i-1} = \mathbf{r}_i - \mathbf{r}_{i-1}$ and $\mathbf{u}_i = \mathbf{r}_{i+1} - \mathbf{r}_i$ from a path with N kinks at positions $\{\mathbf{r}_1, \mathbf{r}_2, ..., \mathbf{r}_N\}$ and move kink i instantaneously to a new position, $\mathbf{r}_i \to \mathbf{r}_i'$, where the new position is determined by the intersection points created by other paths crossing the secant area of the two chosen segments. If there is a single path crossing the secant area at $\mathbf{r}$, then $\mathbf{r}_i' = \mathbf{r}_i + (1 - \epsilon)(\mathbf{r} - \mathbf{r}_i) = \mathbf{r} + \epsilon(\mathbf{r}_i - \mathbf{r})$, where $\epsilon < 1$ is related to chain thickness. If there is no path crossing the secant area, then $\mathbf{r}_i'$ lies on the segment connecting $\mathbf{r}_{i-1}$ and $\mathbf{r}_{i+1}$, and the exact location depends on the method. After such a move, the Z-codes eliminate a kink and end up with $N - 1$ kinks. If there are two or more paths intersecting the secant area, one can artifically introduce kinks until a single intersecting path is left, which is a strategy employed in Z1.

Let us now consider the original annealing method (method A) at very low temperature. In that limit, the velocity $\dot{\mathbf{r}}_i$ of bead i and the force $\mathbf{F}_i$ on it are equivalent, apart from a prefactor, ζ, that has dimensions of an effective friction coefficient. The force acting on bead i is $\mathbf{F}_i = k\mathbf{u}_{i+1} - k\mathbf{u}_i + \mathbf{F}_{\mathrm{EV}}$ where k is the spring coefficient, and $\mathbf{F}_{\mathrm{EV}}$ is the force due to excluded volume interaction. The random noise term disappears at zero-temperature. If there is no bead within the cutoff distance, $\mathbf{F}_{\mathrm{EV}} = 0$, and $\dot{\mathbf{r}}_i = (k/\zeta)(\mathbf{u}_i - \mathbf{u}_{i-1})$. This velocity points in direction of the center $\mathbf{r}_{\mathrm{cm}}$ between $\mathbf{r}_{i+1}$ and $\mathbf{r}_{i-1}$, and $\mathbf{r}_i(t)$ asymptotically (exponentially slowly) reaches this point, i.e., asymptotically agrees with the geometric construction. If there is a single, point-like repulsive interaction site at $\mathbf{r}$, and if we assume a radially symmetrical excluded volume interaction potential, and related force $\mathbf{F}_{\mathrm{EV}}(r)$, we have $\dot{\mathbf{r}}_i = (2k/\zeta)(\mathbf{r}_{\mathrm{cm}} - \mathbf{r}_i) + \mathbf{F}_{\mathrm{EV}}(|\mathbf{r} - \mathbf{r}_i|)$, where $\mathbf{r}_{\mathrm{cm}}$ and $\mathbf{r}$ are fixed. It is understood that $\mathbf{r}_i$ is the point on the path closest to $\mathbf{r}$, i.e. the point with the largest (if any) contribution to the overall excluded volume force. It is sufficient to recognize that the stationary solution of this differential

Table 2. Ensemble-Averaged Properties for the $N = 300$ Case Listed in Table 1 as a Function of Strength of Annealing A[a]

	$A = 0$	$A = 1$	$A = 10$	$A = 16$	$A = 50$	$A = 500$	$A = 10^3$	$A = 10^5$	$A = 10^6$	$A = 10^7$	$A = \infty$
$\langle L_{\mathrm{ppA}}^{(A)} \rangle$	92.9	91.3	85.7	85.4	85.3	85.7	85.6	88.7	93.4	101.7	116.6
$\langle L_{\mathrm{ppA}\to\mathrm{Z}}^{(A)} \rangle$	67.5	67.1	67.2	66.8	66.8	67.0	67.2	69.0	70.9	73.0	74.5

[a] Lengths are reported in lattice units. $\langle L_{\mathrm{ppZ}} \rangle$ for the equilibrated sample is 77.8. The annealing parameter A is varied, while $\tau_{\mathrm{A}} = 10\tau_{\mathrm{R}}$ is held fixed. The two extremes $A = 0$ and $A = \infty$ correspond to the limits where chains can freely disentangle, and where the annealing procedure gets stuck, respectively. Accordingly, for $A = \infty$, results $\langle L_{\mathrm{ppA}\to\mathrm{Z}} \rangle$ and $\langle L_{\mathrm{ppZ}} \rangle$ become very comparable, while $\langle L_{\mathrm{ppA}\to\mathrm{Z}}^{(A \le 1000)} \rangle$ values are close to $\langle L_{\mathrm{ppA}\to\mathrm{Z}}^{(0)} \rangle$, which suggests that the amount of disentanglement in all these cases is comparably large.

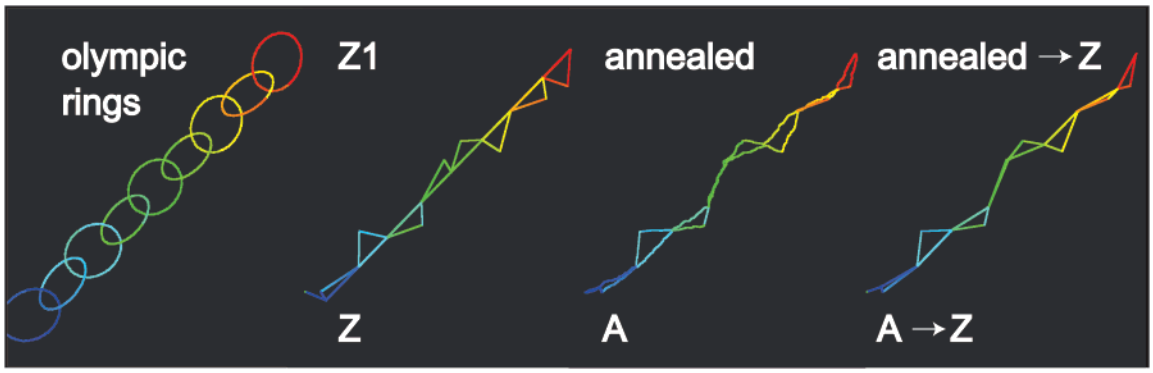

Figure 6. Entanglement networks obtained via annealing, Z1, and annealing followed by Z1 for topologically entangled "olympic rings" on a grid, artificially opened at arbitrarily chosen locations. These locations are easily visible in the Z construction, while slip during the annealing procedure potentially allows to find a shorter path (disentanglement is impossible in this particular example). A → Z mainly preserves the annealed path but straightens it since it does not operate on a grid. Average number of beads on the rings is approximately 190.

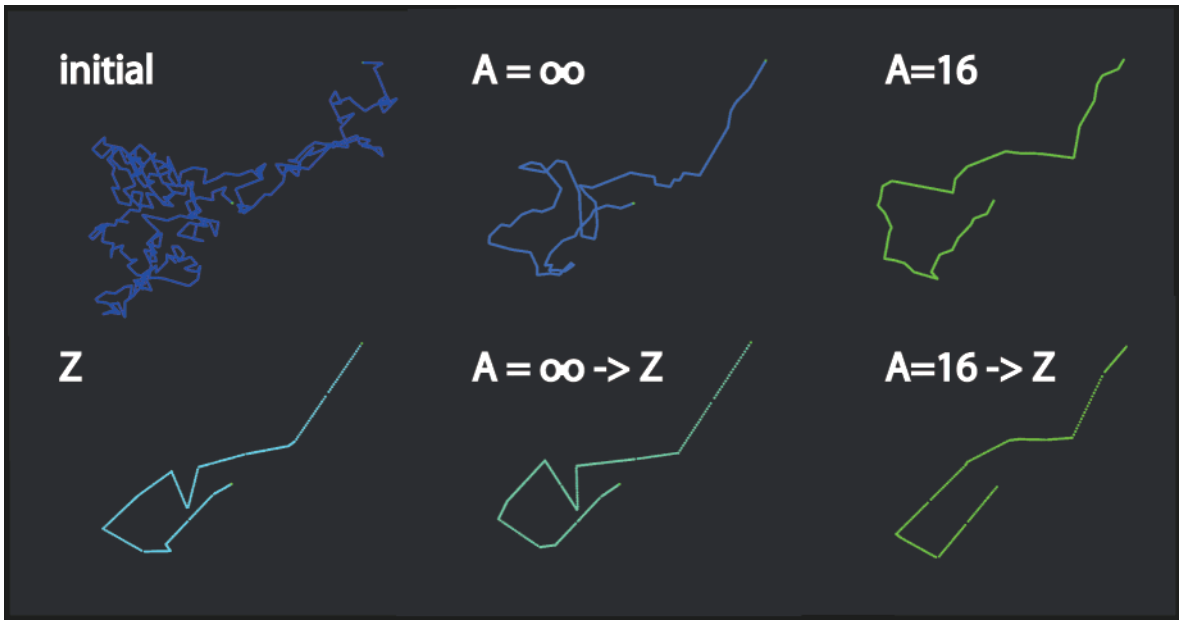

Figure 7. Effect of annealing parameter A on the entanglement network subjected to the Z-code. At least one entanglement, preserved at $A = \infty$, is obviously lost at $A = 16$. Shown is a single chain from the $N = 300$ sample.

equation is the point closest to $\mathbf{r}$ which is attached to the center $\mathbf{r}_{cm}$ by a spring, to understand that the geometric construction is almost equivalent. Other subtle differences, between the geometrical and annealing methods are secondary. The chain thickness parameter ϵ is obviously related to the excluded volume force strength divided by temperature, and density of beads along the polymer contour. To summarize, at infinitely low temperatures, the polymer chains within the annealing approach possess infinitely large friction, and the bead motion is confined to the secant area because the connector between center $\mathbf{r}_{cm}$ and $\mathbf{r}_i$ is fully embedded within the secant area, cf. Figure 8. Thus, if the size of the beads is gradually decreased during zero-temperature annealing, keeping the ratio of the bond-length to bead size the same to prevent chain crossing, it can be seen that the annealing and Z1 algorithms become equivalent.

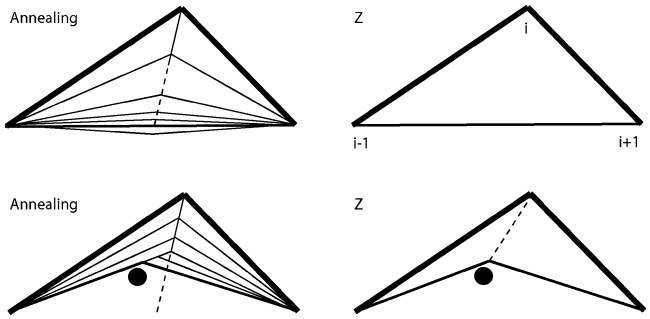

Figure 8. Sketch of specific Annealing and geometric processes (Z-codes) within the secant area of two adjacent segments during minimization in the case of no crosspoints (top row) and a single crosspoint (bottom row). Both methods give very comparable results in the zero temperature limit

Summary and Perspective

Methods to generate PP networks fall into two broad families, annealing and geometrical methods. We critically reviewed and quantitatively compared a lattice-MC based annealing method, and Z1 which is a geometrical method. We observed a 15% discrepancy in the mean PP length obtained by Z1 $\langle L_{ppZ} \rangle$, when the annealed PP network obtained from a equilibrated entangled polymer melt was supplied as input instead of the equilibrated system itself. It illustrated that the entanglement density of the PP network obtained by annealing was smaller than that generated by Z1. We conjectured that end-looping which arises because annealing permits increases in contour length, and chain slip account for the observed discrepancy. Using a toy-system comprising topologically entangled rings, we demonstrated that chain slip acting alone can change network characteristics, even

in the absence of end-looping (or disentanglement). For linear chains it was observed that some entanglements that are preserved when the system is quenched to zero temperature rapidly, are lost during gradual cooling. We argued that the original annealing algorithm becomes equivalent to the geometrical methods when the system is cooled to zero temperature instantaneously, and the size of the beads is gradually shrunk while keeping the ratio of the bond-length to bead size constant.

Unlike molecular dynamics, the S−BFM is a lattice model, and the discrete nature of the lattice introduces error. We have been careful to point out this source of error in this paper and in previous publications. In contrast to MD simulations, the computational cost required to equilibrate long linear chains, or branched polymers using S−BFM is quite small, and could be orders of magnitude smaller. In addition, there has been a surge of interest in hooking up these microscopic and mesoscopic simulations with more coarse-grained models such as beyond equilibrium molecular dynamics,[8,35] and slip-link models.[24,25,29] The bridge between these two levels of modeling is the PP network, which can be generated from mesoscopic simulations and used as the starting point for slip-link models, at least in principle. These slip-link models are coarse-grained at about the 10 nm level, whereas S−BFM is coarse-grained at the Kuhn step or 1 nm level. Thus, the disadvantages of S−BFM attributable mainly to the discretization of space into a lattice are likely to be inconsequential, while the advantages, namely, the speed with which the dynamics or equilibrium structure of a well-entangled system can simulated would be preserved. In addition, S−BFM when used in tandem with Z1 allows us to transition from a lattice to an off-lattice description. This combination, which was demonstrated in this paper, is thus a powerful tool in multiscale modeling of polymer melts.

Acknowledgment. M.K. would like to thank C. Tzoumanekas, R. Hoy, K. Kamio, and K. Moorthi for discussions. This work has been supported by NMP3-CT-2005-016375 and EU Priority FP6-2004-NMP-TI-4 STRP 033339 related grants of the European Community. S.S. would like to thank SCS, COE, and CRC FYAP 07 for financial support.

References and Notes

(1) Doi, M.; Edwards, S. F. *The Theory of Polymer Dynamics*; Clarendon Press: Oxford, U.K., 1986.
(2) McLeish, T. C. B.; Milner, S. T. *Polym. Sci.* **1999**, *143*, 195−256.
(3) Fang, J.; Kröger, M.; Öttinger, H. C. *J. Rheol.* **2000**, *44*, 1293−1317.
(4) Marrucci, G.; Ianniruberto, G. *Macromol. Symp.* **2002**, *185*, 199−210.
(5) Graham, R. S.; Likhtman, A. E.; McLeish, T. C. B.; Milner, S. T. *J. Rheol.* **2003**, *47*, 1171−1200.
(6) Watanabe, H. *Polym. Sci.* **1999**, *24*, 1253−1403.
(7) Kröger, M.; Loose, W.; Hess, S. *J. Rheol.* **1993**, *37*, 1057−1079.
(8) Kröger, M. *Models for Polymeric and Anisotropic Liquids;* Springer: Berlin, 2005.
(9) Hua, C. C.; Schieber, J. D. *J. Chem. Phys.* **1998**, *109*, 10018−10027.
(10) Shanbhag, S.; Larson, R. G.; Takimoto, J.; Doi, M. *Phys. Rev. Lett.* **2001**, *87*, 195502.
(11) Doi, M.; Takimoto, J. *Philos. Trans. R. Soc. London, Ser. A-Math. Phys. Eng. Sci.* **2003**, *361*, 641−650.
(12) Schieber, J. D.; Neergaard, J.; Gupta, S. *J. Rheol.* **2003**, *47*, 213−233.
(13) Tzoumanekas, C.; Theodorou, D. N. *Curr. Opin. Solid State Mater. Sci.* **2007**, doi:10.1016/j.cossms.2006.11.003.
(14) Nair, D. M.; Schieber, J. D. *Macromolecules* **2006**, *39*, 3386−3397.
(15) Mead, D. W. *Rheol. Acta* **2007**, *46*, 369−395.
(16) Masubuchi, Y.; Takimoto, J.-I.; Koyama, K.; Ianniruberto, G.; Marrucci, G.; Greco, F. *J. Chem. Phys.* **2001**, *115*, 4387−4394.
(17) Likhtman, A. E. *Macromolecules* **2005**, *38*, 6128−6139.
(18) Kröger, M. *Phys. Rep.* **2004**, *390*, 453−551.
(19) Everaers, R.; Sukumaran, S. K.; Grest, G. S.; Svaneborg, C.; Sivasubramanian, A.; Kremer, K. *Science* **2004**, *303*, 823−826.
(20) Rubinstein, M.; Helfand, E. *J. Chem. Phys.* **1985**, *82*, 2477−2483.
(21) Shanbhag, S.; Larson, R. G. *Phys. Rev. Lett.* **2005**, *94* (7), 076001.
(22) Kröger, M. *Comput. Phys. Commun.* **2005**, *168*, 209−232.
(23) Tzoumanekas, C.; Theodorou, D. N. *Macromolecules* **2006**, *39*, 4592−4604.
(24) Larson, R. G.; Zhou, Q.; Shanbhag, S.; Park, S. J. *AIChE J.* **2007**, *53*, 542−548.
(25) Shanbhag, S.; Park, S.; Zhou, Q.; Larson, R. *Mol. Phys.* **2007**, in press.
(26) Zhou, Q.; Larson, R. G. *Macromolecules* **2005**, *38*, 5761−5765.
(27) Shanbhag, S.; Larson, R. G. *Macromolecules* **2006**, *39*, 2413−2417.
(28) Sukumaran, S. K.; Grest, G. S.; Kremer, K.; Everaers, R. *J. Polym. Sci., Polym. Phys.* **2005**, *43*, 917−933.
(29) Foteinopoulou, K.; Karayiannis, N.; Mavrantzas, V.; Kröger, M. *Macromolecules* **2006**, *39*, 4207−4216.
(30) Hoy, R. S.; Robbins, M. O. *Phys. Rev. E* **2005**, *72*, 061802.
(31) Carmesin, I.; Kremer, K. *Macromolecules* **1988**, *21*, 2819−2823.
(32) Kröger, M.; Hess, S. *Phys. Rev. Lett.* **2000**, *85*, 1128−1131.
(33) Voigt, H.; Kröger, M. *Macromol. Theory Simul.* **1994**, *3*, 639−647.
(34) Zhou, Q.; Larson, R. *Macromolecules* **2006**, *39*, 6737−6743.
(35) Öttinger, H. *Beyond Equilibrium Thermodynamics;* Wiley: Hoboken, NJ, 2005.
(36) Shaffer, J. S. *J. Chem. Phys.* **1994**, *101*, 4205−4213.

MA062457K